Elsevier Editorial System(tm) for Journal of Process Control
Manuscript Draft

Manuscript Number: JPROCONT-D-14-00203

Title: Anti-slug control solutions based on identified model

Article Type: CAB/DYCOPS 2013

Keywords: Oil production, anti-slug control, unstable systems, robust control

Corresponding Author: Dr. Esmaeil Jahanshahi,

Corresponding Author's Institution:

First Author: Esmaeil Jahanshahi

Order of Authors: Esmaeil Jahanshahi; Sigurd Skogestad, Professor

Abstract: A anti-slug control requires operation around an open-loop unstable operating point. One solution is to design a robust controller based on a mechanistic model. An alternative and more robust approach is to identify an unstable model of the system based on input-output data. We used a closed-loop step test to identify an unstable linear model. From this, we obtained a second order IMC (Internal Model Control) controller that can be implemented as a PIDF controller. From the asymptotes of the proposed IMC controller, we also derive a simple tuning for PI-controller. Next, we considered two types of robust H-infinity controller (mixed-sensitivity and loop-shaping). The proposed model identification and control solutions were verified experimentally on two different test rigs. We found that the robustness and performance of the IMC (PIDF) controller is comparable with the H-infinity controllers. However, the prosed IMC (PIDF) controller is easier to tune compared to H-infinity control.

Highlights

May 8, 2014

The paper includes the following contributions:

- We present new PIDF and PI tuning rules for anti-slug control at offshore oilfields.
- We propose to identify a second-order unstable model from a closed-loop step test.
- Model identification and tuning rules are tested experimentally.
- Agreement between identified and mechanistic models is surprisingly good.
- Performance and robustness of PIDF controller is comparable with $\mathcal{H}_\infty$ controllers.

Anti-slug control solutions based on identified model

Esmaeil Jahanshahi, Sigurd Skogestad

Department of Chemical Engineering, Norwegian University of Science and Technology (NTNU), NO-7491 Trondheim (e-mail: skoge@ntnu.no)

Abstract

A anti-slug control requires operation around an open-loop unstable operating point. One solution is to design a robust controller based on a mechanistic model. An alternative and more robust approach is to identify an unstable model of the system based on input-output data. We used a closed-loop step test to identify an unstable linear model. From this, we obtained a second order IMC (Internal Model Control) controller that can be implemented as a PIDF controller. From the asymptotes of the proposed IMC controller, we also derive a simple tuning for PI-controller. Next, we considered two types of robust $\mathcal{H}_\infty$ controller (mixed-sensitivity and loop-shaping). The proposed model identification and control solutions were verified experimentally on two different test rigs. We found that the robustness and performance of the IMC (PIDF) controller is comparable with the $\mathcal{H}_\infty$ controllers. However, the prosed IMC (PIDF) controller is easier to tune compared to $\mathcal{H}_\infty$ control.

Keywords: Oil production, anti-slug control, unstable systems, robust control
2014 MSC: JPROCONT-S-14-00286

1. Introduction

Severe slugging flow regimes usually occur in pipeline-riser systems that transport oil and gas mixture from the seabed to the surface (Yocum (1973)). Such flow regimes, also referred to as "riser slugging", are characterised by severe flow and pressure oscillations. Slugging problems have also been observed in gas-lifted oil wells where two types of instabilities, casing heading and density wave instability, have been reported (e.g. Hu and Golan (2003)). See Aamo et al. (2005) for more references on gas-lift instability.

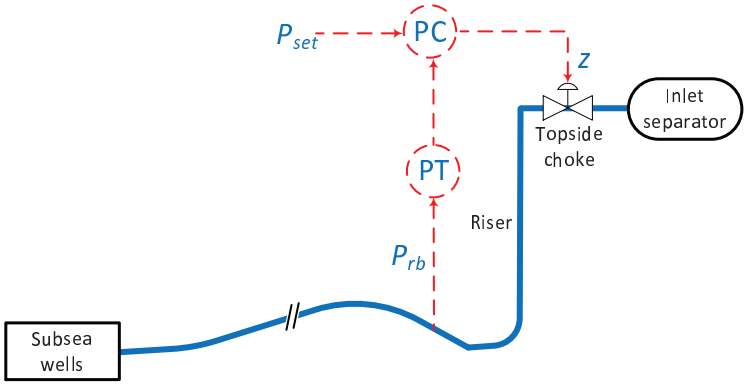

Figure 1: Preventing slug flow by control of riser base pressure ($MV = Z$, $CV = P_{rb}$)

Slugging has been recognised as a serious problem in offshore oilfields, because the irregular flow caused by slugging can cause serious operational problems for the downstream surface facilities (e.g. overflow of inlet separators). Therefore, effective ways to handle or remove riser slugging are needed, and many efforts have been made in order to prevent such occurrences (Courbot (1996), Havre et al. (2000)). The conventional solution is to reduce the opening of the top-side choke valve (choking), but this may reduce the production rate especially for fields where the reservoir pressure is relatively low. Therefore, a solution that guarantees stable flow together with the maximum possible production rate is desirable.

Fortunately, automatic feedback control has been shown to be an effective strategy to eliminate the slugging problem (Havre et al. (2000), Godhavn et al. (2005)). As shown in Figure 1, the top-side choke valve is usually used as the manipulated variable to regulate (control) the riser base pressure (P_{rb}) at a given pressure set-point (P_{set}). Such a system is referred to as 'anti-slug control' and it aims at stabilising the flow in the pipeline at operating conditions that, without control, would lead to riser slugging.

However, existing anti-slug control systems are not robust and tend to become unstable after some time, because of inflow disturbances or plant changes. The main objective of our research is to design robust anti-slug control systems. The nonlinearity of the system is one problem for a linear controller, because the gain of the system changes drastically at different operating conditions. In addition, the effective time delay is another problematic factor for stabilization.

One solution is to use nonlinear model-based controllers to counteract the nonlinearity (e.g.

Di Meglio et al. (2010)). However, we have found that these solutions are less robust against time delays or plant/model mismatch (Jahanshahi and Skogestad (2013b)).

An alternative approach is to identify an unstable model of the system, for example, using a closed-loop step test. We use the identified model for an IMC (Internal Model Control) design, which in our case can be realized as a PIDF controller. We define a PIDF controller as

$$K_{PIDF}(s) = K_c \left(1 + \frac{1}{sT_i} + \frac{T_d s}{T_f s + 1}\right) \tag{1}$$

where K_p is the proportional gain, T_i is the integral time, T_d is the derivative time and T_f is the time constant of the derivative action filter. We differentiate this from a PID controller (with a filter), because the low-pass filter a crucial part of the controller for our application, not just to reduce the noise effect. That is we cannot set T_f to a small value and obtain the same or better performance.

As the simpler alternative solution, we consider PI-control, which is the preferred choice in the industry. However, appropriate settings are required for robustness, and we obtain the PI-controller settings from the asymptotes of the proposed IMC controller.

Finally, we consider two different robust $\mathcal{H}_\infty$ controllers. First, we use an $\mathcal{H}_\infty$ mixed-sensitivity design which minimizes $\overline{\sigma}(S)$ for performance, $\overline{\sigma}(T)$ for robustness and low sensitivity to noise, and $\overline{\sigma}(KS)$ to penalize large inputs. Next, we use $\mathcal{H}_\infty$ loop-shaping design where we specify an initial controller (plant loop shape), and apply a loop-shaping procedure that improves the robustness by maximizing the stability margin (Skogestad and Postlethwaite (2005)). The PIDF controller was used to form the initial loop shape. The results provided in this paper have been partially presented by Jahanshahi and Skogestad (2013a), and Jahanshahi et al. (2014).

This paper is organized as follows. Section 2 describes the pipeline-riser system. The closed-loop model identification is introduced in Section 3, the new PIDF tuning is presented in Section 4, and the simple PI-tuning is introduced in Section 5. Mixed-sensitivity and loop-shaping designs are presented in Section 6 and Section 7, respectively. Small-scale and Medium-scale experiments are presented in Section 8 and Section 9. Finally, we summarize the main conclusions and remarks in Section 10 and Section 11.

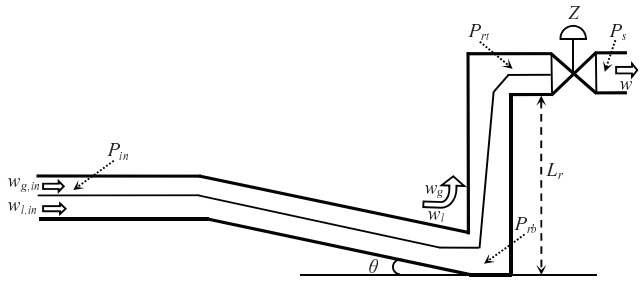

Figure 2: Schematic presentation of pipeline-riser system

2. Systems description

Figure 2 shows a schematic presentation of the system. The inflow rates of gas and liquid to the system, $w_{g,in}$ and $w_{l,in}$, are assumed to be independent disturbances and the top-side choke valve opening ($0 < Z < 100\%$) is the manipulated variable. A fourth-order dynamic model for this system was presented by Jahanshahi and Skogestad (2011). The state variables of this model are as:

- m_{gp}: mass of gas in pipeline [kg]
- m_{lp}: mass of liquid in pipeline [kg]
- m_{gr}: mass of gas in riser [kg]
- m_{lr}: mass of liquid in riser [kg]

The four state equations of the model are

$$\dot{m}_{gp} = w_{g,in} - w_g \tag{2}$$

$$\dot{m}_{lp} = w_{l,in} - w_l \tag{3}$$

$$\dot{m}_{gr} = w_g - \alpha w \tag{4}$$

$$\dot{m}_{lr} = w_l - (1-\alpha) w \tag{5}$$

The flow rates of gas and liquid from the pipeline to the riser, w_g and w_l, are determined by virtual valve equations from the pressure drop across the riser-base. The outlet mixture flow rate, w, is determined by the relative opening ($Z\,[\%]$) of the top-side choke valve. The flow rates mentioned

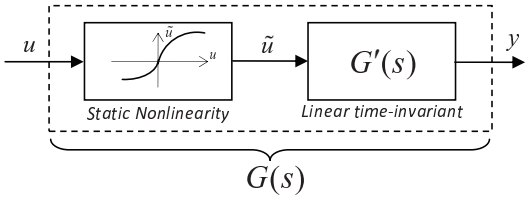

Figure 3: Block diagram for Hammerstein model

above and the gas mass fraction, α, in the equations (2)-(5) are calculated by additional model equations given by Jahanshahi and Skogestad (2011).

However, Jahanshahi and Skogestad (2013a) found that a second-order linear model with two unstable poles and one stable zero is enough for the control design purposes. Such a model can be identified by a closed-loop step test, and this method is explained in the following.

3. Model identification

To include nonlinear effects, we use a Hammerstein model structure (Figure 3) to describe the desired unstable operating point (flow regime). The Hammerstein model consists of a series connection of a static nonlinearity (gain K) and a linear time-invariant dynamic system, $G'(s)$.

For identification of the unstable dynamics, we need to assume a structure. We first considered a simple unstable first-order plus delay model:

$$G(s) = \frac{Ke^{-\theta s}}{\tau s - 1} = \frac{be^{-\theta s}}{s - a} \tag{6}$$

where $a > 0$ and $K = b/a$ represents the static nonlinearity. If we control this system with a proportional controller with gain K_{c0} (Figure 4), the closed-loop transfer function from the set-point (y_s) to the output (y) becomes

$$\frac{y(s)}{y_s(s)} = \frac{K_{c0}G(s)}{1 + K_{c0}G(s)} = \frac{K_{c0}be^{-\theta s}}{s - a + K_{c0}be^{-\theta s}}. \tag{7}$$

In order to get a stable closed-loop system, we need $K_{c0}b > a$. The steady-state gain of the closed-loop transfer function is always larger than 1,

$$\frac{\Delta y_\infty}{\Delta y_s} = \frac{K_{c0}b}{K_{c0}b - a} > 1. \tag{8}$$

However, the closed-loop experimental step response (see Figure 5) shows that the closed-loop steady-state gain is smaller than one. Therefore, the model form in (6) is not correct.

To get the correct model form, we linearize the four-state mechanistic model in Section 2 around the desired unstable operating point, and we get a fourth-order linear model in the form

$$G(s) = \frac{\theta_1(s+\theta_2)(s+\theta_3)}{(s^2-\theta_4 s+\theta_5)(s^2+\theta_6 s+\theta_7)}. \tag{9}$$

This model contains two unstable poles, two stable poles and two zeros. Seven parameters (θ_i) must be estimated to identify this model. However, if we look at the Hankel Singular Values of the fourth-order model (Figure 6), we find that the stable part of the system has little dynamic contribution. This suggests that a model with two unstable poles is sufficient for control design. Using model truncation (square root method), we obtained a reduced-order model in the form

$$G(s) = \frac{b_1 s + b_0}{s^2 - a_1 s + a_0}, \tag{10}$$

where $a_0 > 0$ and $a_1 > 0$. The model has two unstable poles and four parameters, b_1, b_0, a_1 and a_0, need to be estimated. If we control the unstable process in (10) using a proportional controller with gain K_{c0}, the closed-loop transfer function from set-point (y_s) to output (y) becomes

$$\frac{y(s)}{y_s(s)} = \frac{K_{c0}(b_1 s + b_0)}{s^2 + (-a_1 + K_{c0}b_1)s + (a_0 + K_{c0}b_0)}. \tag{11}$$

This can be rewritten to the model used by Yuwana and Seborg (1982):

$$\frac{y(s)}{y_s(s)} = \frac{K_2(1+\tau_z s)}{\tau^2 s^2 + 2\zeta\tau s + 1}, \tag{12}$$

where K_2 must be less than one as found experimentally. To estimate the four parameters (K_2, τ_z, τ and ζ) in (12), we use a very simple approach where we read six key parameters (Δy_p, Δy_u, Δy_∞, Δy_s, t_p and t_u) from the experimental closed-loop response (see Figure 5). Having the closed-loop stable model in (12), we can back-calculate the parameters of the open-loop unstable model in (10). Details are given in Appendix A.

4. New PIDF tuning based on IMC design

4.1. IMC design for unstable systems

The Internal Model Control (IMC) design procedure is summarized by Morari and Zafiriou (1989). The block diagram of the IMC structure is shown in Figure 7. Here, $G(s)$ is the nominal

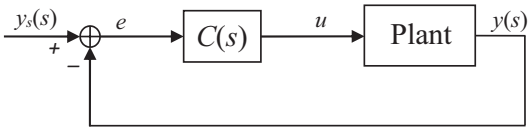

Figure 4: Closed-loop system with conventional feedback. In the experimental step test we use $C(s) = K_{c0}$

.

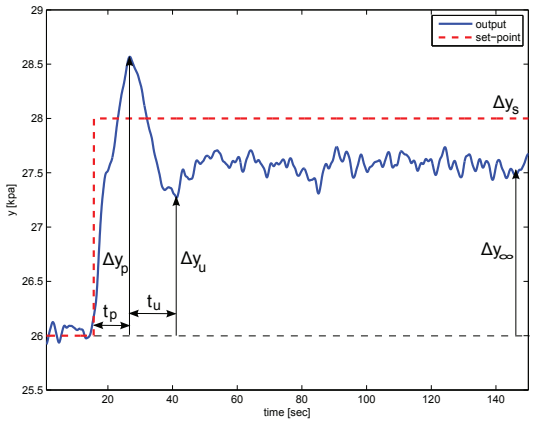

Figure 5: Experimental closed-loop step response for system stabilized with proportional control

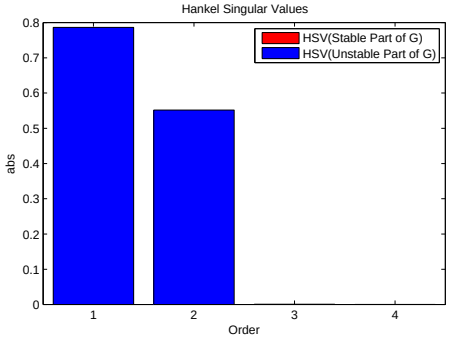

Figure 6: Hankel Singular Values of fourth order model

model which in general has some mismatch with the real plant $G_p(s)$. $\tilde{Q}(s)$ is the inverse of the minimum phase part of $G(s)$ and $f(s)$ is a low-pass filter for robustness of the closed-loop system.

The IMC configuration in Figure 7 cannot be used directly for unstable systems; instead we use the conventional feedback structure with the stabilizing controller

$$C(s) = \frac{\tilde{Q}(s)f(s)}{1 - G(s)\tilde{Q}(s)f(s)}. \tag{13}$$

For internal stability, $\tilde{Q}f$ and $(1 - G\tilde{Q}f)$ have to be stable. We use the identified model with two unstable poles and one stable zero in (10) as the plant model:

$$G(s) = \frac{\hat{b}_1 s + \hat{b}_0}{s^2 - \hat{a}_1 s + \hat{a}_0} = \frac{k'(s+\varphi)}{(s-\pi_1)(s-\pi_2)} \tag{14}$$

and we get

$$\tilde{Q}(s) = \frac{(1/k')(s-\pi_1)(s-\pi_2)}{s+\varphi} \tag{15}$$

We design the filter $f(s)$ as explained by Morari and Zafiriou (1989):

k = number of RHP poles + 1 = 3

m = max(number of zeros of $\tilde{Q}(s)$ - number of pole of $\tilde{Q}(s)$,1) = 1 (to make $Q = \tilde{Q}f$ proper)

n = m + k -1 = 3 (filter order)

With $n = 3$, the filter is in the following from:

$$f(s) = \frac{\alpha_2 s^2 + \alpha_1 s + \alpha_0}{(\lambda s + 1)^3}, \tag{16}$$

where λ is the adjustable closed-loop time-constant. We choose $\alpha_0 = 1$ to get integral action and the coefficients α_1 and α_2 are calculated by solving the following system of linear equations:

$$\begin{pmatrix} {\pi_1}^2 & \pi_1 & 1 \\ {\pi_2}^2 & \pi_2 & 1 \end{pmatrix} \begin{pmatrix} \alpha_2 \\ \alpha_1 \\ \alpha_0 \end{pmatrix} = \begin{pmatrix} (\lambda\pi_1 + 1)^3 \\ (\lambda\pi_2 + 1)^3 \end{pmatrix} \tag{17}$$

Finally, from (13) the feedback version of the IMC controller becomes

$$C(s) = \frac{[\frac{1}{k'\lambda^3}](\alpha_2 s^2 + \alpha_1 s + 1)}{s(s+\varphi)}. \tag{18}$$

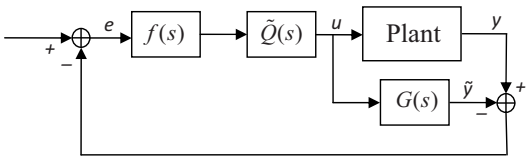

Figure 7: Block diagram of Internal Model Control system

4.2. PIDF implementation of IMC controller

Here, we obtain PIDF settings from the proposed IMC controller. The IMC controller in (18) is a second order transfer function which can be written in form of a PID controller with a low-pass filter.

$$K_{PIDF}(s) = K_c \left(1 + \frac{1}{sT_i} + \frac{T_d s}{T_f s + 1}\right) \tag{19}$$

where

$$T_f = 1/\varphi \tag{20}$$

$$T_i = \alpha_1 - T_f \tag{21}$$

$$K_c = \frac{T_i T_f}{k' \lambda^3} \tag{22}$$

$$T_d = \frac{\alpha_2}{T_i} - T_f \tag{23}$$

For the controller work in practice, we require that $K_c < 0$ and $T_d > 0$; and we must choose λ such that these two conditions are satisfied. This was observed in the experiments.

5. PI-controller tuning

Next, we consider PI control. There are many approaches to get tuning values for PI control. For example, relay-feedback auto-tuning has been used by Ogazi et al. (2009) for PI tuning based on a first-order unstable model. Here, we obtain the PI tuning based on the IMC controller from the previous Section. We consider a PI controller in the following form

$$K_{PI}(s) = K_c \left(1 + \frac{1}{\tau_I s}\right), \tag{24}$$

The PIDF controller in (19) can be approximated by a PI-controller by considering the high- and low-frequency asymptotes of $C(s)$ in (18).

$$K_c = \lim_{s \to \infty} C(s) = \frac{\alpha_2}{k' \lambda^3} \tag{25}$$

$$\tau_I = \frac{K_c}{\lim\limits_{s\to 0} sC(s)} = \alpha_2 \varphi \tag{26}$$

6. $\mathcal{H}_\infty$ mixed-sensitivity design

We consider an $\mathcal{H}_\infty$ problem where we want to bound $\overline{\sigma}(S)$ for performance, $\overline{\sigma}(T)$ for robustness and low sensitivity to noise, and $\overline{\sigma}(KS)$ to penalize large inputs. These requirements may be combined into a stacked $\mathcal{H}_\infty$ problem (Skogestad and Postlethwaite (2005)).

$$\min_K \|N(K)\|_\infty, \quad N \triangleq \begin{bmatrix} W_u KS \\ W_T T \\ W_P S \end{bmatrix} \tag{27}$$

where W_u, W_T and W_P determine the desired shapes of KS, T and S, respectively. Typically, W_P^{-1} is chosen to be small at low frequencies to achieve good disturbance attenuation (i.e., performance), and W_T^{-1} is chosen to be small outside the control bandwidth, which helps to ensure good stability margin (i.e., robustness). W_u is often chosen as a constant. The solution to this optimization problem gives a stabilizing controller K that satisfies (Doyle et al. (1989), Glover and Doyle (1988)):

$$\begin{aligned} \overline{\sigma}(KS(j\omega)) &\le \gamma \underline{\sigma}(W_u^{-1}(j\omega)) \\ \overline{\sigma}(T(j\omega)) &\le \gamma \underline{\sigma}(W_T^{-1}(j\omega)) \\ \overline{\sigma}(S(j\omega)) &\le \gamma \underline{\sigma}(W_P^{-1}(j\omega)) \end{aligned} \tag{28}$$

y_2 is the particular output for feedback control in the generalized plant in Figure 8. The value of γ in equation (28) should be as small as possible for good controllability. However, it depends on the design specifications W_u, W_T and W_P.

7. $\mathcal{H}_\infty$ loop-shaping design

We consider the stabilization of the plant G which has a normalized left coprime factorization

$$G = M^{-1}N \tag{29}$$

where we have dropped the subscripts from M and N for simplicity. A perturbed plant model G_p can then be written as

$$G_p = (M + \Delta_M)^{-1}(N + \Delta_N) \tag{30}$$

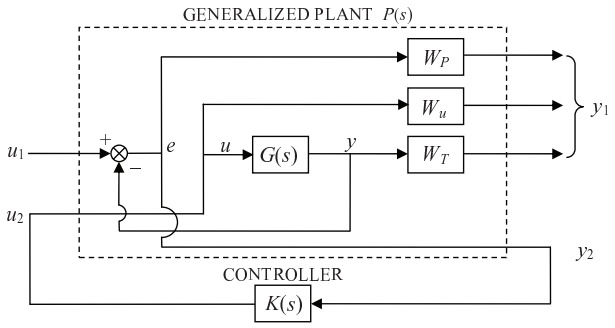

Figure 8: Closed-loop system for mixed sensitivity control design

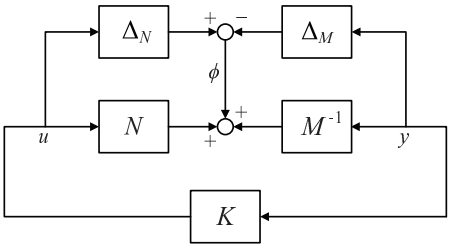

Figure 9: $\mathcal{H}_\infty$ robust stabilization problem

where Δ_M and Δ_N are stable unknown transfer functions which represent the uncertainty in the nominal plant model G. The objective of robust stabilization is to stabilize not only the nominal model G, but a family of perturbed plants defined by

$$G_p = \left\{(M + \Delta_M)^{-1}(N + \Delta_N) : \|[\Delta_N \;\; \Delta_M]\|_\infty < \epsilon\right\} \tag{31}$$

where $\epsilon > 0$ is then the stability margin (Skogestad and Postlethwaite (2005)). To maximize this stability margin is the problem of robust stabilization of normalized coprime factor plant description as introduced and solved by Glover and McFarlane (1989).

For the perturbed feedback system of Figure 9, the stability property is robust if and only if the nominal feedback system is stable and

$$\gamma_K \triangleq \left\| \begin{bmatrix} K \\ I \end{bmatrix} (I - GK)^{-1} M^{-1} \right\|_\infty \leq \frac{1}{\epsilon} \tag{32}$$

Notice that γ_K is the $\mathcal{H}_\infty$ norm from ϕ to $\begin{bmatrix} u \\ y \end{bmatrix}$ and $(I - GK)^{-1}$ is the sensivity function for this positive feedback arragmenet. A samll γ_K is corresponding to a large stability margin.

8. Small-scale experiments

8.1. Exprimental setup

The experiments were performed on a small-scale laboratory rig for anti-slug control at the Chemical Engineering Department of NTNU. Figure 10 shows a schematic presentation of the laboratory setup. The pipeline and the riser are made from flexible pipes with 2 cm inner diameter. The length of the pipeline is 4 m, and it is inclined with a 15° angle. The height of the riser is 3 m. A buffer tank is used to simulate the effect of a long pipe with the same volume, such that the total resulting length of pipe would be about 70 m.

The topside choke valve opening Z is used as the input for control ($MV = Z$). The separator pressure after the topside choke valve is nominally constant at atmospheric pressure. The feed into the pipeline is assumed to be at constant flow rates, 4 $litre/min$ of water and 4.5 $litre/min$ of air. With these boundary conditions, the critical valve opening where the system switches from stable (non-slug) to oscillatory (slug) flow is at $Z^* = 15\%$ for the top-side valve. The bifurcation diagrams are shown in Figure 11.

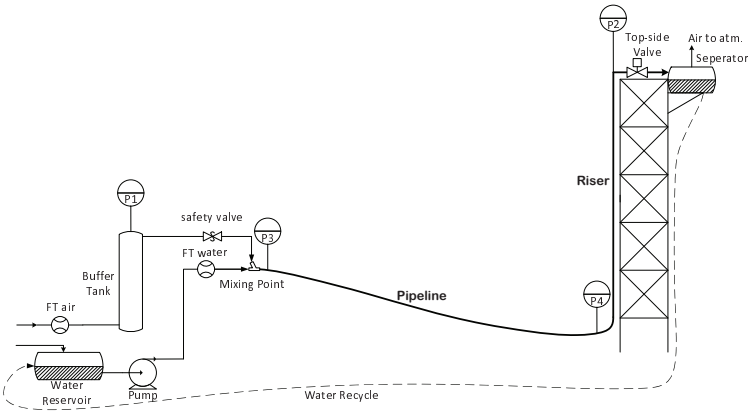

Figure 10: Small-scale experimental rig

The desired steady-state (dashed middle line) at slugging conditions ($Z > 15\%$) is unstable, but it can be stabilized using feedback control. The slope of the steady-state line (in the middle) is the static gain of the system, $k = \partial y/\partial u = \partial P_{in}/\partial Z$. As the valve opening increase this slope decreases, and the gain finally approaches zero. This makes control of the system with large valve openings very difficult. On the other hand, large valve openings are desirable because this minimizes the pressure drop over the valve and increases the production rate.

The controlled output in experiments is the inlet pressure of the pipeline ($CV = P_{in}$). As mentioned above stabilizing the system at large valve openings (low pressure set-points) is difficult because of the small gain. We decrease the controller set-point to see if the controller can stabilize the system with lower set-point. we use the same set of descending pressure set-points in all experiments. The controllers are tuned (designed) for a valve opening of $Z = 30\%$, and controllers with good gain margin can stabilize the system with larger valve openings (lower set-points). To have an impartial comparison for robustness of the controllers, we tune the controllers such that all of them result in the same input usage ($M_{ks} = 50$). Here, M_{ks} is peak of KS and for the PIDF controller in (19) it becomes

$$M_{ks} = -K_c(T_d/T_f + 1). \tag{33}$$

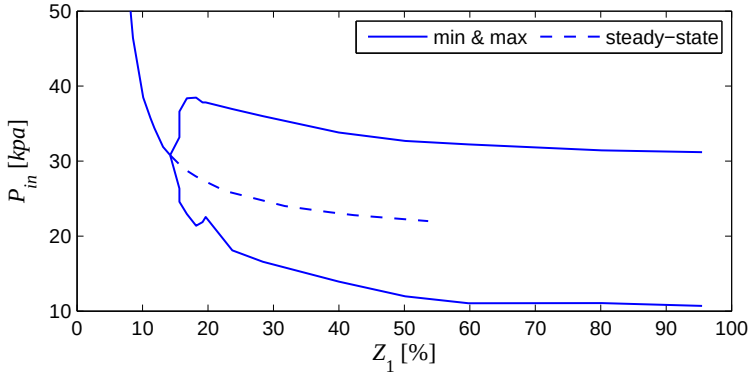

Figure 11: Experimental bifurcation diagrams for small-scale rig

8.2. Model identification

Valve opening of $Z = 20\%$

The flow regime switches to slugging flow at a valve opening of $Z = 15\%$, hence it is unstable at $Z = 20\%$. We closed the loop with a proportional controller with $K_{c0} = -10$, and changed the set-point by 2 *kPa* (Figure 12). Since the response is noisy, a low-pass filter was used to reduce the noise effect. Then, we use the method described in Section 3 to identify the closed-loop stable transfer function:

$$\frac{y(s)}{y_s(s)} = \frac{3.13s + 0.81}{20.62s^2 + 2.20s + 1} \tag{34}$$

The identified closed-loop transfer function is shown by the red line in Figure 12. From this, we back-calculate to an open-loop unstable process model:

$$G(s) = \frac{-0.015(s + 0.26)}{s^2 - 0.045s + 0.0093} \tag{35}$$

If we linearize the four-state mechanistic model given in (2)-(5) at the operating point $Z = 20\%$, we get the following fourth-order model.

$$G(s) = \frac{-0.28(s + 20.21)(s + 0.27)}{(s^2 - 0.046s + 0.013)(s^2 + 21.68s + 256.1)} \tag{36}$$

The frequency response of the identified model at the valve opening $Z = 20\%$ (35) is compared to the mechanistic model (36) in Figure 13. This agreement is surprisingly good. The two unstable poles of the mechanistic model are $p = 0.0233 \pm 0.1096i$, and the unstable poles of the identified model are $p = 0.0227 \pm 0.0937i$.

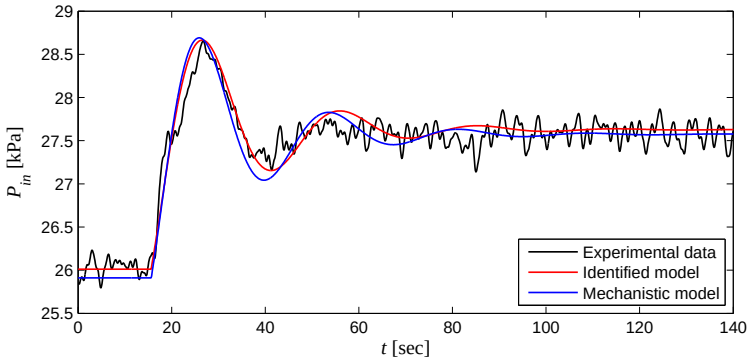

Figure 12: Experimental closed-loop step test compared with identified model and mechanistic model ($Z = 20\%$)

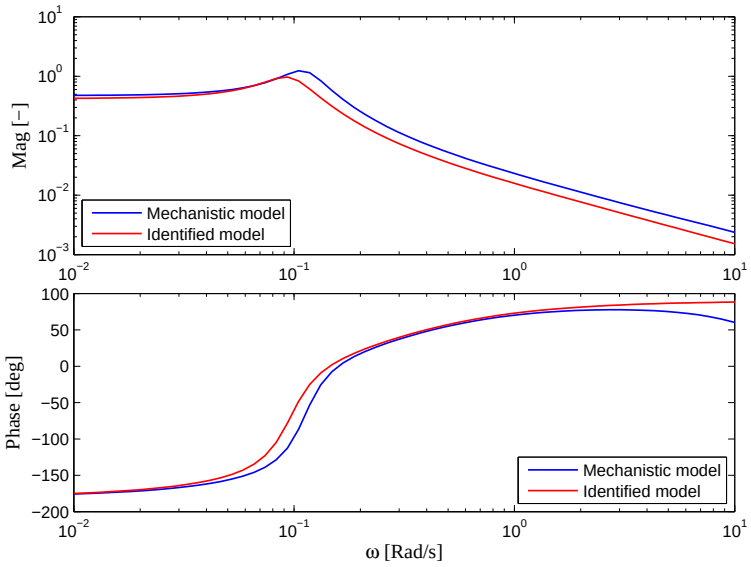

Figure 13: Comparison of identified and mechanistic models in frequency domain ($Z = 20\%$)

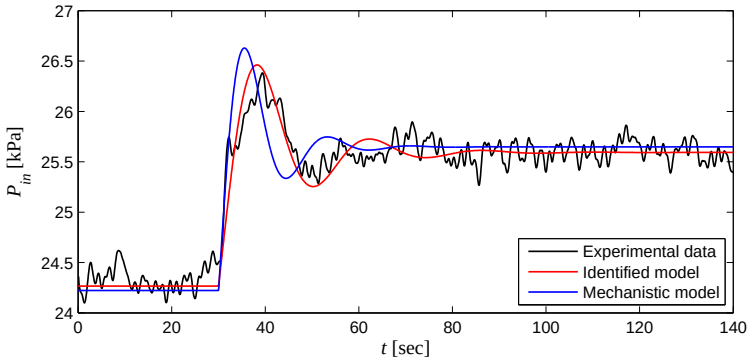

Figure 14: Experimental closed-loop step test compared with identified model and mechanistic model ($Z = 30\%$)

Valve opening of $Z = 30\%$

We repeated the previous experiment at $Z = 30\%$ valve opening. We closed the loop using a proportional controller with $K_{c0} = -20$ and changed the set-point by 2 kPa (Figure 14). Then, we use the method explained in Section 3 to identify the closed-loop stable transfer function:

$$\frac{y(s)}{y_s(s)} = \frac{2.634s + 0.6635}{13.39s^2 + 2.097s + 1} \tag{37}$$

The identified closed-loop transfer function is shown by the red line in Figure 14. Then, we back-calculate to an open-loop unstable system:

$$G(s) = \frac{-0.0098(s + 0.25)}{s^2 - 0.04s + 0.025} \tag{38}$$

The four-state mechanistic model given in (2)-(5), linearized at the operating point $Z = 30\%$, results in the following fourth-order model.

$$G(s) = \frac{-0.18(s + 20.18)(s + 0.27)}{(s^2 - 0.17s + 0.023)(s^2 + 26.57s + 303.4)} \tag{39}$$

The frequency response of the identified model at the valve opening $Z = 30\%$ (38) is compared to the mechanistic model (39) in Figure 15. The agreement is very good also in this case. The two unstable poles of the mechanistic model are $p = 0.0860 \pm 0.1235i$, and the two poles of the identified model are $p = 0.0200 \pm 0.1572i$.

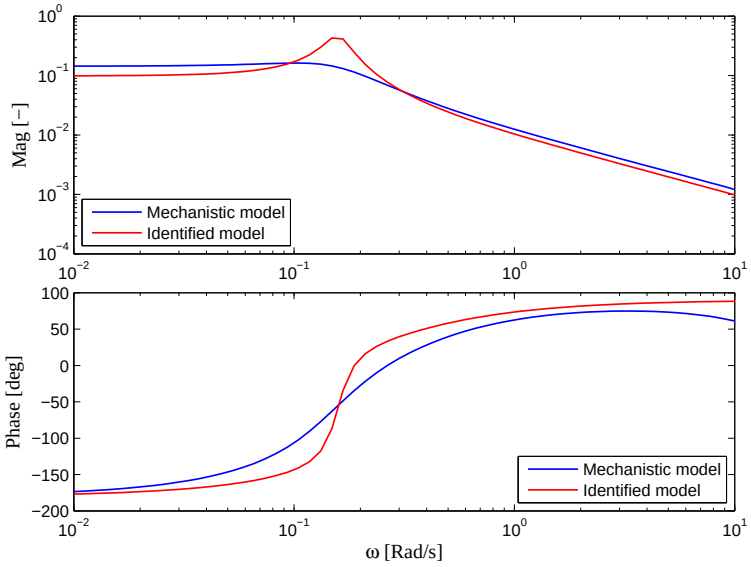

Figure 15: Comparison of identified and mechanistic models in frequency domain ($Z = 30\%$)

8.3. IMC (PIDF)

We used the identified model in (38) for an IMC design. We chose the filter time constant $\lambda = 6.666\ s$ to get $M_{ks} = 50$. The resulting IMC controller becomes

$$C(s) = \frac{-50(s^2 + 0.0867s + 0.0069)}{s(s + 0.25)}. \tag{40}$$

Note that the controller has complex zeros. The corresponding PIDF setting values are $K_c = -11.84$, $T_i = 8.59\,s$, $T_d = 12.89\,s$ and $T_f = 4\,s$. Figure 16 shows performance of the PIDF controller in the experiment. It was stable with 2 *sec* added time delay.

8.4. PI tuning

Next, we obtain the PI tuning from the IMC controller (40) as explained in Section 5. The PI tuning parameters are $K_c = -50.00$ and $\tau_I = 36.30\,s$. Figure 17 shows result of experiment using the PI controller. This controller was stable with 1 *sec* added time delay.

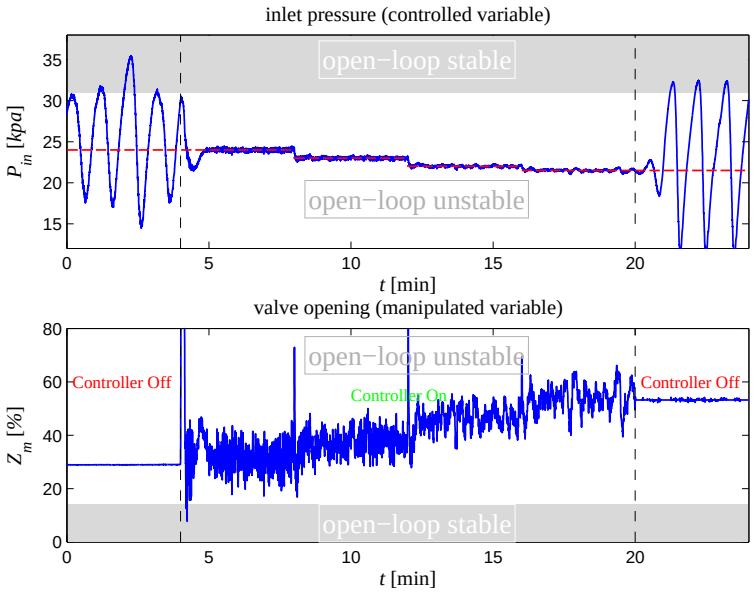

Figure 16: Experimental result of PIDF with $K_c = -11.84$, $T_i = 8.59\,s$, $T_d = 12.89\,s$ and $T_f = 4\,s$

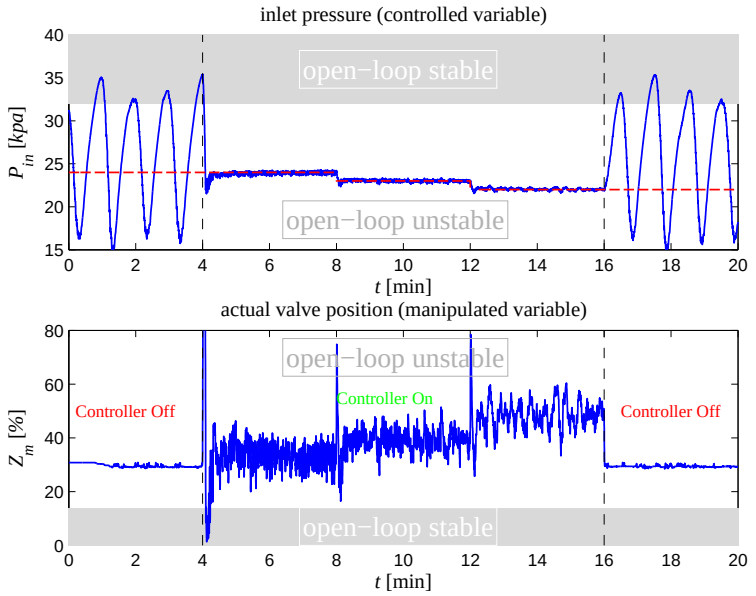

Figure 17: Experimental result of PI controller with $K_c = -50.00$, $\tau_I = 36.30\,s$

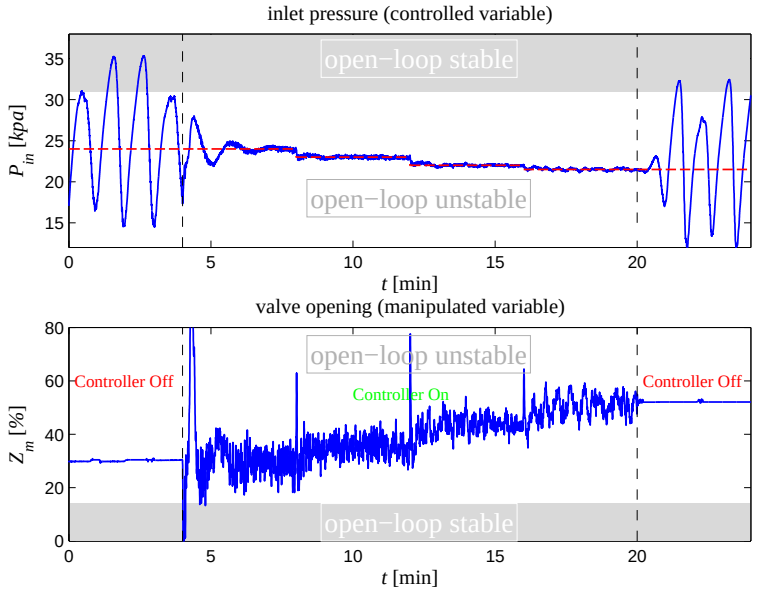

Figure 18: Experimental result of loop-shaping $\mathcal{H}_\infty$

8.5. $\mathcal{H}_\infty$ loop-shaping

We used the IMC controller (40) to obtain the initially shaped plant for the $\mathcal{H}_\infty$ loop-shaping design. The following fifth-order controller was resulted.

$$C(s) = \frac{-188.49(s^2 + 0.02s + 0.005)(s^2 + 0.087s + 0.0069)}{s(s + 0.25)(s + 3.76)(s^2 + 0.082s + 0.0067)} \tag{41}$$

The experimental result of the controller in (41) is shown in Figure 18.

8.6. $\mathcal{H}_\infty$ mixed-sensitivity

We design the $\mathcal{H}_\infty$ mixed-sensitivity controller with the following design specifications:

$$W_P(s) = \frac{s/M_s + \omega_B}{s + \omega_B A}, \tag{42}$$

$$W_T(s) = \frac{s/(10\omega_B) + 1}{0.01s + 1}, \tag{43}$$

$$W_u = 0.0135, \tag{44}$$

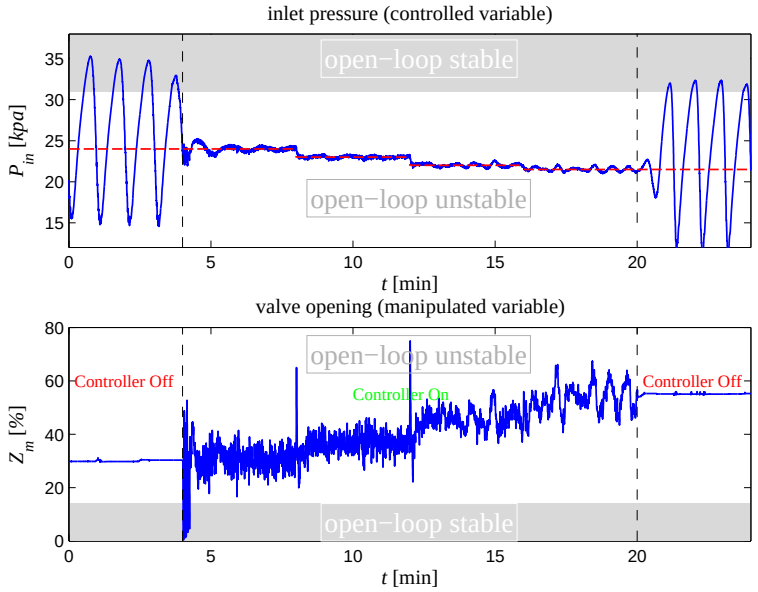

Figure 19: Experimental result of mixed-sensitivity $\mathcal{H}_\infty$

where $M_s = 1$, $\omega_B = 0.14$ and $A = 0.01$. We chose these design specifications so that we achieve $M_{ks} = 50$ and good robustness properties. We get the following fourth-order stabilizing controller.

$$C(s) = \frac{-9.08\times10^6(s+100)(s^2+0.0137s+0.011)}{(s+1.8\times10^5)(s+112.5)(s+0.231)(s+0.0014)} \tag{45}$$

We achieved $\gamma = 1.21$ with this controller; the experimental performance is shown in Figure 19.

9. Medium-scale experiments

9.1. Experimental setup

The tuning procedures were validated also on a medium-scale test rig. This test rig is an S-riser with a height of about 7 *m*. Other dimensions of this experimental set-up are shown in Figure 20. This riser is made from stainless steel pipes with inner diameter of 50 *mm*. Similar to the small scale setup, an air buffer thank is installed at inlet to emulate the effect of a long pipeline with the same volume. The volume of the buffer tank is 200 litres; this is equivalent 101.86 *m* of pipe. The inlet flow rates to the system are 0.0024 *kg/sec* air and 0.3927 *kg/sec* water. The outlet separator

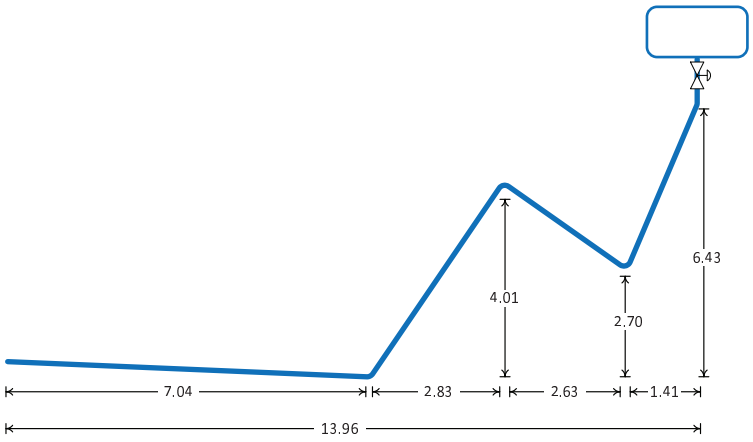

Figure 20: Experimental setup for medium-scale S-riser rig, all dimensions in *meter*

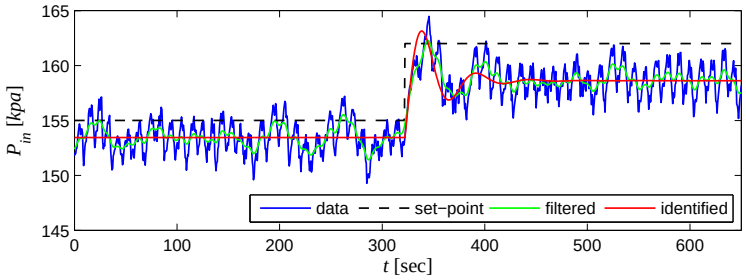

Figure 21: Closed-loop step test on medium-scale rig

pressure is constant at the atmospheric pressure. With these boundary conditions, the system switches from non-slug to slugging flow conditions at $Z^* = 16\%$ opening of the topside valve.

9.2. IMC (PIDF) controller at Z=18%

Figure 21 shows a closed-loop step test performed on the S-riser. A proportional controller with the gain $K_{c0} = -250$ was used for the test. The pressure set-point before the step test was 155 kPa which results in a valve opening of $Z = 18\%$ (region of unstable open-loop operation). We identified an unstable model as the following:

$$G(s) = \frac{-5.6 \times 10^{-4}(s + 0.082)}{s^2 - 0.069s + 0.0040} \tag{46}$$

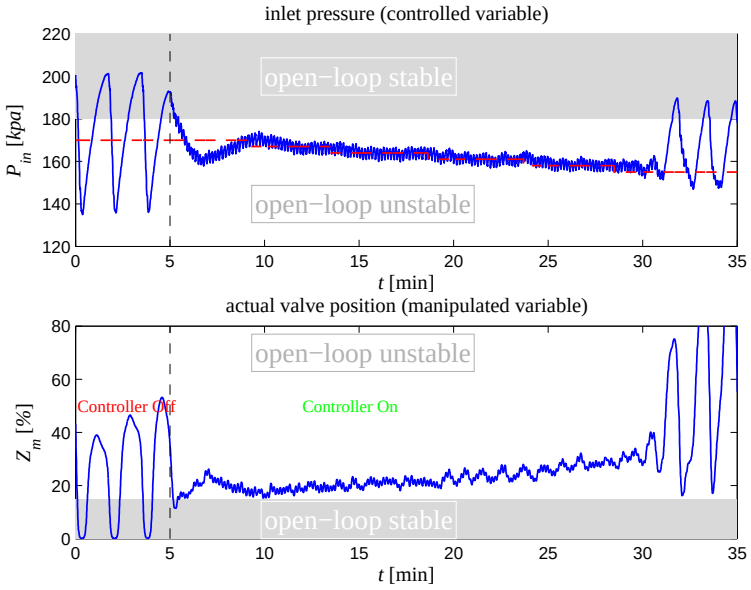

Figure 22: Experimental result of PIDF controller with $K_c = -3.47$, $T_i = 2.33\,s$, $T_d = 1.19 \times 10^4\,s$ and $T_f = 12.25\,s$ on medium-scale rig

By choosing $\lambda = 24.5$, we designed the following IMC controller:

$$C(s) = \frac{-340.75(s^2 + 0.0052s + 0.00036)}{\mathrm{s(s + 0.0816)}} \tag{47}$$

The corresponding PIDF tuning are $K_c = -3.47$, $T_i = 2.33\,s$, $T_d = 1.19 \times 10^4\,s$ and $T_f = 12.25\,s$. Experimental result of control using this PIDF tuning is shown in Figure 22. In this experiment, we decreased the set-point until the system becomes unstable. This controller was able to control the system up to a $Z = 32\%$ valve opening, which is two time of the critical valve opening $Z^* = 16\%$.

9.3. PI-controller tuning at Z=18%

The PI tuning obtained from the IMC controller in (47) are $K_c = -340.75$ and $\tau_I = 229.23\,s$. The experimental result is given in Figure 23 where system was stabilized up to $Z = 24\%$.

10. Discussion

Performance and robustness of the different controllers used in the experiments are compared in Table 1. We use Integral Square Error (ISE) as a measure of the performance, and the robustness

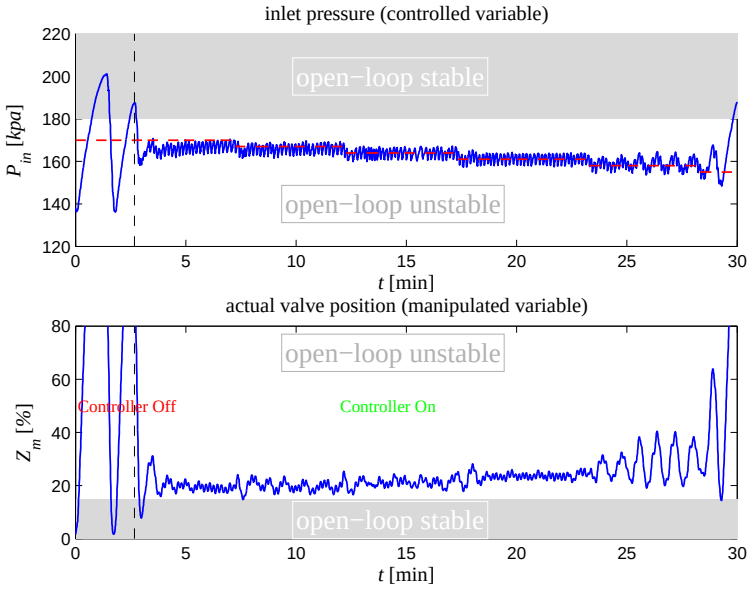

Figure 23: Experimental result of PI controller with $K_c = -340.75$ and $\tau_I = 229.23\,s$ on medium-scale rig

is evaluated based on peak of T, gain-margin and delay-margin. The PIDF controller shows the best performance, and the PI controller is the second best controller for performance. The $\mathcal{H}_\infty$ mixed-sensitivity controller shows a large value for ISE, because for the lower set-points it has some oscillations (see Figure 19). This is related to the poor gain-margin of the controller; the $\mathcal{H}_\infty$ mixed-sensitivity has the largest (worst) value for the gain-margin. The $\mathcal{H}_\infty$ loop-shaping controller has the best gain-margin, and the smallest value for the peak of T. On the other hand, The $\mathcal{H}_\infty$ mixed-sensitivity has the best delay-margin, but the worst gain margin as mentioned.

In summary, considering combined performance and robustness measures, the $\mathcal{H}_\infty$ loop-shaping controller is the best, and the PIDF controller is the next one in our results.

11. Conclusion

In this paper we developed and compared feedback controllers for unstable multiphase flow in risers. The study included simple PIDF tuning rules, PI-tuning and two $\mathcal{H}_\infty$ controllers. The comparison was based on experimental tests carried out in two prototype flow systems.

Table 1: Comparison of different controllers in experiments

Controller	ISE	$\|S\|_\infty$	$\|T\|_\infty$	$\|KS\|_\infty$	GM	DM
IMC PIDF	171.45	1.00	1.19	50	0.11	2.49
IMC PI	178.03	1.03	1.38	51.64	0.10	1.80
$\mathcal{H}_\infty$ Loop Shaping	184.98	1.10	1.12	50	0.10	2.48
$\mathcal{H}_\infty$ Mixed Sensitivity	330.25	1.00	1.18	50	0.15	3.00

We identified a second-order unstable model for the system, and compared the identified model with a mechanistic model in time domain and the frequency domain. The identified model for a valve opening of 20% is very close to the mechanistic model. Also, agreement between the models for a valve opening of 30% was good.

We showed that for this case performance and robustness of a PIDF controller is close to $\mathcal{H}_\infty$ controllers (see Table 1). Slightly better results can be achieved by the $\mathcal{H}_\infty$ loop-shaping approach, where we employ the PIDF controller to obtain the initially shaped plant. However, this method results in higher order controllers which may not be desired by the practitioner.

The $\mathcal{H}_\infty$ mixed-sensitivity design is more involved as it requires tuning of many weights simultaneously. However, we could not achieve better results than that of a PIDF controller for this case and further investigation is needed.

We tested the PIDF and PI controllers on a medium-scale flow system which shows applicability of the proposed tuning rules on large systems. Testing the tuning rules in real applications is recommended.

We have used three PIDF controllers in a gain-scheduling scheme to counteract the nonlinearity over wide operation range (from 20% to 60% valve opening). Compared to nonlinear controllers based on the mechanistic model, the gain-scheduling solution is more robust, and it does not need the mechanistic model (Jahanshahi and Skogestad (2013b)).

Acknowledgements

Funding for this research was provided by SIEMENS, Oil and Gas Solutions. The medium-scale experiment were carried out at the multi-phase laboratory, Department of Energy and Process

Engineering (EPT). We would like to thank professor Ole Jørgen Nydal for providing us this opportunity. We also acknowledge help from Mahnaz Esmaeilpour, the master student who carried out the medium-scale experiments.

References

Aamo, O., Eikrem, G., Siahaan, H., and Foss, B. (2005). Observer design for multiphase flow in vertical pipes with gas-lift - theory and experiments. *Journal of Process Control*, 15(3), 247 – 257.

Courbot, A. (1996). Prevention of severe slugging in the dunbar 16 inches multiphase pipeline. In *Proceedings of the Annual Offshore Technology Conference*, volume 4, 445–452. *SPE no.* 8196.

Di Meglio, F., Kaasa, G.O., Petit, N., and Alstad, V. (2010). Model-based control of slugging flow: an experimental case study. In *American Control Conference*, 2995–3002. Baltimore, USA.

Doyle, J., Glover, K., Khargonekar, P., and Francis, B. (1989). State-space solutions to standard $\mathcal{H}_2$ and $\mathcal{H}_\infty$ control problems. *IEEE Transactions on Automatic Control*, 34(8), 831–847.

Glover, K. and Doyle, J.C. (1988). State-space formulae for all stabilizing controllers that satisfy an $\mathcal{H}_\infty$-norm bound and relations to relations to risk sensitivity. *Systems and Control Letters*, 11(3), 167–172.

Glover, K. and McFarlane, D. (1989). Robust stabilization of normalized coprime factor plant descriptions with h_∞-bounded uncertainty. *IEEE Transactions on Automatic Control*, 34(8), 821–830.

Godhavn, J.M., Fard, M.P., and Fuchs, P.H. (2005). New slug control strategies, tuning rules and experimental results. *Journal of Process Control*, 15, 547–557.

Havre, K., Stornes, K., and Stray, H. (2000). Taming slug flow in pipelines. *ABB Review*, 4, 55–63.

Hu, B. and Golan, M. (2003). Gas-lift instability resulted production loss and its remedy by feedback control: dynamical simulation results. In *SPE International Improved Oil Recovery Conference in Asia Pacific*, 513–521. SPE no. 84917-MS, Kuala Lumpur, Malaysia.

Jahanshahi, E. and Skogestad, S. (2011). Simplified dynamical models for control of severe slugging in multiphase risers. In *18th IFAC World Congress*, 1634–1639. Milan, Italy.

Jahanshahi, E., de Oliveira, V., Gimholt, C., and Skogestad, S. (2014). A comparison between internal model control pidf, optimal pidf and robust controllers for unstable flow in risers. In *19th IFAC World Congress*. Cape Town, South Africa.

Jahanshahi, E. and Skogestad, S. (2013a). Closed-loop model identification and pid/pi tuning for robust anti-slug control. In *10th IFAC International Symposium on Dynamics and Control of Process Systems*. Mumbai, India.

Jahanshahi, E. and Skogestad, S. (2013b). Comparison between nonlinear modelbased controllers and gain-scheduling internal model control based on identified model. In *52nd IEEE Conference on Decision and Control*. Florence, Italy.

Morari, M. and Zafiriou, E. (1989). *Robust Process Control*. Prentice Hall, Englewood Cliffs, New Jersey.

Ogazi, A., Ogunkolade, S., Cao, Y., Lao, L., and Yeung, H. (2009). Severe slugging control through open loop unstable pid tuning to increase oil production. 17–32.

Skogestad, S. and Postlethwaite, I. (2005). *Multivariable Feedback Control: Analysis and Design*. Wiley & Sons, Chichester, West Sussex, UK.

Yocum, B. (1973). Offshore riser slug flow avoidance: Mathematical models for design and optimization. In *SPE European Meeting*, SPE no. 4312–MS. Society of Petroleum Engineers, London, United Kingdom.

Yuwana, M. and Seborg, D.E. (1982). A new method for on-line controller tuning. *AIChE Journal*, 28(3), 434–440.

Appendix A. Model Identification Calculations

Stable closed-loop transfer function:

$$\frac{y(s)}{y_s(s)} = \frac{K_2(1+\tau_z s)}{\tau^2 s^2 + 2\zeta\tau s + 1} \tag{A.1}$$

The Laplace inverse (time-domain) of the transfer function in (A.1) is given in Yuwana and Seborg (1982) as

$$y(t) = \Delta y_s K_2 \left[1 + D \exp(-\zeta t/\tau) \sin(Et + \phi)\right], \tag{A.2}$$

where

$$D = \frac{\left[1 - \frac{2\zeta\tau_z}{\tau} + \left(\frac{\tau_z}{\tau}\right)^2\right]^{\frac{1}{2}}}{\sqrt{1-\zeta^2}} \tag{A.3}$$

$$E = \frac{\sqrt{1-\zeta^2}}{\tau} \tag{A.4}$$

$$\phi = \tan^{-1}\left[\frac{\tau\sqrt{1-\zeta^2}}{\zeta\tau - \tau_z}\right] \tag{A.5}$$

By differentiating (A.2) with respect to time and setting the derivative equation to zero, one gets time of the first peak:

$$t_p = \frac{\tan^{-1}\left(\frac{1-\zeta^2}{\zeta}\right) + \pi - \phi}{\sqrt{1-\zeta^2}/\tau} \tag{A.6}$$

And the time between the first peak (overshoot) and the undershoot:

$$t_u = \pi\tau/\sqrt{1-\zeta^2} \tag{A.7}$$

The damping ratio ζ can be estimated as

$$\hat{\zeta} = \frac{-\ln v}{\sqrt{\pi^2 + (\ln v)^2}} \tag{A.8}$$

where

$$v = \frac{\Delta y_\infty - \Delta y_u}{\Delta y_p - \Delta y_\infty} \tag{A.9}$$

Then, using equation (A.7) we get

$$\hat{\tau} = \frac{t_u\sqrt{1-\hat{\zeta}^2}}{\pi}. \tag{A.10}$$

The steady-state gain of the closed-loop system is estimated as

$$\hat{K}_2 = \frac{\Delta y_\infty}{\Delta y_s}. \tag{A.11}$$

We use time of the peak t_p and (A.6) to get an estimate of ϕ :

$$\hat{\phi} = \tan^{-1}\left[\frac{1-\hat{\zeta}^2}{\hat{\zeta}}\right] - \frac{t_p\sqrt{1-\hat{\zeta}^2}}{\hat{\tau}} \tag{A.12}$$

From (A.4), we get

$$\hat{E} = \frac{\sqrt{1-\hat{\zeta}^2}}{\hat{\tau}} \tag{A.13}$$

The overshoot is defined as

$$D_0 = \frac{\Delta y_p - \Delta y_\infty}{\Delta y_\infty}. \tag{A.14}$$

By evaluating (A.2) at time of peak t_p we get

$$\Delta y_p = \Delta y_s \hat{K}_2 \left[1 + \hat{D}\exp(-\hat{\zeta}t_p/\hat{\tau})\sin(\hat{E}t_p + \hat{\phi})\right] \tag{A.15}$$

Combining equation (A.11), (A.14) and (A.15) gives

$$\hat{D} = \frac{D_0}{\exp(-\hat{\zeta}t_p/\hat{\tau})\sin(\hat{E}t_p + \hat{\phi})}. \tag{A.16}$$

We can estimate the last parameter by solving (A.3):

$$\hat{\tau}_z = \hat{\xi}\hat{\tau} + \sqrt{\hat{\zeta}^2\hat{\tau}^2 - \hat{\tau}^2\left[1 - \hat{D}^2(1-\hat{\zeta}^2)\right]} \tag{A.17}$$

Then, we back-calculate to parameters of the open-loop unstable model. The steady-state gain of the open-loop model is

$$\hat{K} = \frac{\Delta y_\infty}{K_{c0}\left|\Delta y_s - \Delta y_\infty\right|} \tag{A.18}$$

From this, we can estimate the four model parameters in equation (A.5) are

$$\hat{a}_0 = \frac{1}{\hat{\tau}^2(1 + K_{c0}\hat{K}_p)} \tag{A.19}$$

$$\hat{b}_0 = \hat{K}_p\hat{a}_0 \tag{A.20}$$

$$\hat{b}_1 = \frac{\hat{K}_2\hat{\tau}_z}{K_{c0}\hat{\tau}^2} \tag{A.21}$$

$$\hat{a}_1 = -2\hat{\zeta}/\hat{\tau} + K_{c0}\hat{b}_1, \tag{A.22}$$

where $\hat{a}_1 > 0$ gives an unstable system.